27. G. Ohanessian and W. A. Goddard III, *Acc. Chem. Res.* **23**, 386 (1990); C. W. Bauschlicher Jr. and S. R. Langhoff, *Int. Rev. Phys. Chem.* **9**, 149 (1990).
28. J. D. Whitehead, *J. Atmos. Terr. Phys.* **20**, 49 (1961).
29. Following (*34*), balancing the Lorentz force and the rate of ion-neutral collisions gives $e\mathbf{v}_i \times \mathbf{B} = m_i\nu_{in}(\mathbf{v}_i - \mathbf{v}_n)$, where $\mathbf{v}_i$ and $\mathbf{v}_n$ are the ion and neutral velocity vectors. Solving for the vertical component of ion velocity yields $w_i = (u \cos I \cos D)/\eta_i$ for $u \gg v, w$, the meridional and vertical components of the neutral wind, and $\eta_i \gg 1$. Differentiating with respect to $\mathbf{z}$,

$$\frac{\partial w_i}{\partial \mathbf{z}} = \cos I \cos D\left(\frac{\partial u}{\partial z} + \frac{u}{H_n}\right)\Big/\eta_i$$

where H_n is the scale height of the neutral atmosphere. The expressions $\nu_{in} = 2\pi(\alpha_{in}e^2/\mu_{in})^{1/2}\,n$ and $\Omega = eB/m_i$ are from (*6*).
30. The upward wind is usually attributed to $\mathbf{E} \times \mathbf{B}$ drift; in this case, the magnitude of the electric field (*E*) component perpendicular to *B* and *z* is $E_\perp \approx w_i B/\cos I = 0.1$ mV m^{-1}. Similar calculations have been made for Saturn's ionosphere [T. Majeed and J. C. McConnell, *Planet. Space Sci.* **39**, 1715 (1991)].
31. B. Sicardy, P. Goldreich, F. Roques, *Bull. Am. Astron. Soc.* **24**, 963 (1992); F. Roques *et al.*, *Astron. Astrophys.* **288**, 985 (1994).
32. A detailed discussion of gravity waves, including a time-dependent (propagating) wind field, will be present elsewhere (J. R. Lyons, in preparation).
33. K. Noll and the Hubble Space Telescope Team, *Int. Astron. Union Circ. 6038* (1994).
34. S. Kirkwood and P. N. Collis, *J. Atmos. Terr. Phys.* **51**, 259 (1989); W. A. Bristow and B. J. Watkins, *Geophys. Res. Lett.* **18**, 404 (1991).
35. Discussions with G. Lindal, E. R. Kursinski, J. Connerney, Y. Yung, W. Goddard, T. Rebold, and S. Asmar are gratefully acknowledged. G. Lindal provided the electron number density profile. This work was supported by NASA grants NAGW-2362 and NAGW-1509. Contribution 5418 from the Division of Geological and Planetary Sciences, California Institute of Technology.

29 July 1994; accepted 1 November 1994

Stress-Induced Vortex Line Helixing Avalanches in the Plastic Flow of a Smectic A Liquid Crystal

Richard A. Herke,* Noel A. Clark,† Mark A. Handschy

Dynamic surface force measurements of the response of a smectic A to layer normal stress exhibited time dependence for topological events in which single smectic layers were added or removed. Single layer–sized jumps in sample thickness had a rapid component of duration of ~1 second that produced most of the change in separation, but that was heralded by a slow precursor acceleration in separation, which began up to a few hundred seconds before. This avalanche-like dynamic signature is consistent with a relaxation mechanism based on the Glaberson-Clem-Bourdon instability of vortex lines (screw dislocations) in the smectic order parameter.

Smectic A's are liquid crystal phases having rod-shaped molecules organized into a one-dimensional (1D) stack of planar two-dimensional (2D) liquidlike layers, as shown in Fig. 1A. This hybrid 1D solid–2D liquid structure produces a variety of exotic elastic, hydrodynamic, and thermal effects (*1*). One of the most interesting of these is the phenomenon of oscillatory plastic flow, observed when the liquid crystal is confined between solid surfaces in a spherical wedge formed by the crossed cylinders of a surface force apparatus (SFA) (Fig. 1A). In response to the application of a constant rate of layer strain, the smectic A can exhibit oscillatory layer normal stress, apparently the result of events in which single molecular layers are either added or removed (*2–4*). These events are similar to those observed in isotropic liquids when confinement of the liquid between two closely spaced solid surfaces induces layering (*5*). We present here a study of the dynamics and mechanism of single layer jump events.

Condensed Matter Laboratory, Department of Physics, University of Colorado, Boulder, CO 80309, USA.

*Present address: Liquid Crystal Institute, Kent State University, Kent, OH 44242, USA.
†To whom correspondence should be addressed.

Such layering events are intrinsically topological in nature, which can be seen with the smectic A–superconductor–superfluid analogy of de Gennes (*1, 6*) in which the smectic A layering is described by the two-component order parameter $\Psi(\mathbf{r}) = |\Psi(\mathbf{r})|e^{i\phi(\mathbf{r})}$. Here $|\Psi(\mathbf{r})|$ gives the local magnitude of the layering density wave, and the phase $\phi(\mathbf{r})$ advances by 2π on traversing a layer (where $\mathbf{r}$ is position). In the SFA, a constant $\phi(\mathbf{r})$ boundary condition is imposed on each solid surface so that changes in the layer number, for example, $n \rightarrow n - 1$ as in Fig. 1A, correspond to phase slippages of $\phi(\mathbf{r})$. Phase slippage with $\phi(\mathbf{r})$ fixed on the boundary must necessarily be mediated by vortex lines, the topological singularities of the field $\Psi(\mathbf{r})$. In the smectic A these are edge or screw dislocations (*7*). Although the nonuniform gap between the cylinders requires the presence of edge dislocations, our analysis indicates that in the macroscopic limit studied here (closest spacing of the cylinders, d_{min}, >2 μm), they are pinned and not involved in the layer jumps in a significant way.

This leaves screw dislocations to mediate the layering events, and the avalanche-like dynamic signature found in our experiments is consistent with a relaxation mechanism based on the Glaberson *et al.* (*8*)–Clem (*9*)–Bourdon *et al.* (*10*) helical instability of vortex lines found in $\Psi(\mathbf{r})$ systems. The helical instability of screwlike vortex lines was first discovered by Glaberson *et al.* while they were studying the effect of net fluid flow on quantized vortex lines in superfluid Helium II (*8*), and by Clem (*9*), who calculated the response to applied current of vortex flux lines in a type II superconductor. Bourdon *et al.* (*10*) showed that in a smectic A under either compressive or dilative strain, a previously straight screw dislocation line deforms into a helix to eliminate or add layers, respectively. Using the Oswald-Kléman analysis of this instability in the smectic A (*11*), we generated a computer simulation of the collective behavior of an array of screw dislocations under strain and found that a cascade of screw dislocation helixing instabilities did indeed reproduce the principal dynamic features that we observed.

As is typical in SFA studies, our sample, 4′-*n*-octyl-4-cyanobiphenyl (8CB) (*12*), was contained in a spherical wedge made from crossed molecularly smooth cylindrical surfaces of radius *R* and closest spacing d_{min}, with $d_{min} \ll R$. Layering jumps are observable for d_{min} as large as several microns in 8CB (*1*). We used a SFA of our design that enabled us to dynamically measure the force and surface separation (*13*). The cylindrical surfaces ($R = 1.2$ cm) were overlaid with thin pieces of mica (*2–5*), which were then coated with a monolayer of hexadecyltrimethylammonium bromide (HTAB) to provide a smooth surface that enforces homeotropic orientation (layers parallel to the surfaces). Motion of each of the surfaces was detected with a differential capacitance micrometer of sensitivity ~0.05 Å and an absolute accuracy ~10%. The position of the lower cylinder was servo controlled with a piezoelectric stack in conjunction with the capacitance micrometer. The upper cylinder was also attached to a spring of spring constant $K = 2.1 \times 10^7$ dynes/cm, which was mechanically in series with the effective spring of the liquid crystal layer between the cylinders, but which had a much smaller spring constant at low applied force. Displacement sensitivity was limited by electronic noise in the servo to ~ 0.02 Å over short time periods and by mechanical relaxation of ~0.2 Å/min over long periods. The time resolution of the SFA was intrinsically limited to ~0.03 s by the damping due to air flow in the capacitors and to ~0.4 s by analog-to-digital conversion. The SFA was contained in a temperature-controlled oven.

Data collection began with the placement of a drop of the smectic A 8CB in the gap between the cylinders. The surfaces were then brought into "contact," defined as the condition under which they begin to move in unison even when the force F is large. This was sufficient to establish $d_{min} = 0$ for the present experiments which were carried out at relatively large separations, with d_{min} in the range of 0.5 to 4 μm. Forces large enough to begin plastic flow were applied, pulling the lower surface out to make d_{min} about twice as large as desired, and then the surfaces were compressed to the desired separation. The system was allowed to relax for ~1 day before a data run. The lower surface was then raised (or lowered) in very small, discrete steps usually of from 10 to 80 Å, and the displacement of the upper surface to this step was observed for a few minutes. The response was strongly temperature-dependent. The 8CB exhibited a second-order (or very weak first-order) nematic to smectic A phase transition at temperature T_c = 33.7°C (*14–16*), below which the 1D density modulation of the smectic A appeared. Near the transition, the applied stress quickly relaxed, probably through edge dislocation climb, with a time constant τ that increased rapidly with decreasing T, in qualitative agreement with observations in other smectic A materials near a second-order nematic–smectic A transition (*17, 18*). For $T <$ 30°C, this relaxation became extremely slow (τ ~ hours to days), and a new relaxation process appeared, examples of which are plotted in Fig. 1 (obtained at T = 26.5°C, which is 5°C below the nematic–smectic A phase transition in our sample).

When the force was sufficiently small, the response of the upper cylinder was simply to move with nearly the same displacement as the lower cylinder, with the liquid crystal acting as a spring of effective constant K_{LC}, much greater than K:$K_{LC} > 2 \times 10^8$ dynes/cm ~ 10K. The typical time dependence of such a displacement is illustrated for times $t < 0$ in Fig. 1B, which shows the upper surface displacement versus time in response to two compressive steps that followed a series of earlier steps (*19*) which compressed the liquid crystal to $F \sim 1 \times 10^2$ dynes. The upper surface displacement, which after a step was nearly the change in the cylinder separation $\delta d(t)$, was read out with no overshoot in a response time of ~1 s. After the first step, the cylinders began moving back together with the slow, constant background velocity $v_b = \delta d/\delta t \sim$ 0.024 Å/s, which was proportional to the force that preceded the step, a result of the slow relaxation process discussed above. Because K was small compared with K_{LC}, it took many steps to approach F_c, the threshold force of plastic flow. Each of the steps shown in Fig. 1B increased F by only ~4%. After the last step shown (at t = 0 in Fig. 1B) F exceeded F_c (which increases with decreasing d), and the liquid crystalline structure could no longer support F. The surfaces initially moved in unison, but in this case the 4% increase in F substantially increased $\delta d/\delta t$ to ~0.1 Å/s (about four times larger than that of the previous step) immediately after the step. The $\delta d/\delta t$ continued to gradually increase over a period of ~50 s at which time there began a rapidly increasing acceleration to an event that squeezed out a layer, which took ~1 s. This event was completed after a gradual deceleration back to a steady constant $\delta d/\delta t \sim$ 0.012 Å/s during an interval of a few hundred seconds. The net change in cylinder separation through the event, δd, was δd ~32 Å and corresponded well to the bulk smectic A layer thickness a = 31.7 Å (*2*) (distance indicated in Fig. 1B) (*14*). Thus, it appears that a single layer was removed from the sample during this event, which released ~7 dynes, that is, only ~7% of F. Because each relaxation event released only a small fraction of F, it took very few additional compressive steps of the lower surface to induce another similar relaxation event. We found $F_c \sim 1/d_{min}$, possibly a result of an increase in the area of homeotropically ordered 8CB as d_{min} was decreased.

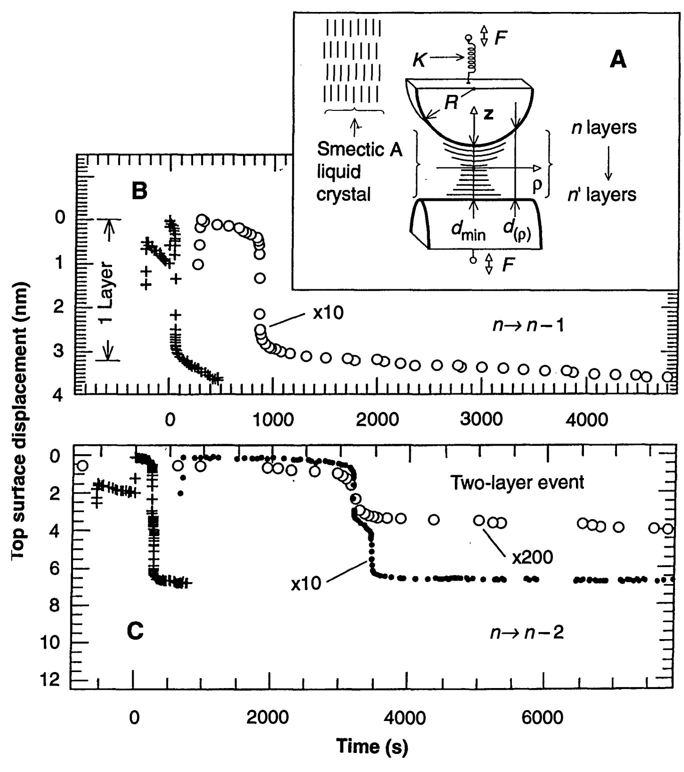

Fig. 1. (**A**) Schematic of the experimental geometry. (**B** and **C**) Examples of movement of the upper cylinder in response to step displacement of the lower cylinder with smectic A liquid crystal 8CB at T = 26.5°C homeotropically aligned (layers parallel to the surfaces) between the cylinders. The examples are of a (B) single layer and (C) consecutive single layer discrete avalanche-like events after the indicated initial step response to the displacement of the lower cylinder. For (B), d_{min} = 4 μm (+); two consecutive compressive steps with a single layer squeezing-out event after the second step, which we take to be at t = 0. The curve of open circles (○) is a ×10 expansion of the t axis after the step, with the start displaced for clarity. For (C), d_{min} = 2.5 μm (+); two consecutive single layer squeezing-out events after a compressive step. The curve of black circles (●) is a ×10 expansion of the t axis, showing a 200-s-long monotonic increase in acceleration antecedent to the layer jump. The curve of open circles (○) is a ×200 expansion of the t axis, showing that the majority of the layer jump occurs in less than 1 s.

Examples of two types of events at T = 26.5°C are shown in Fig. 1, B and C, which uses several magnifications in time to indicate the broad range of time scales over which the events occurred. An example of an event in which two layers were squeezed out is shown in Fig. 1C. Such multiple-step events occurred more often at smaller d_{min}. In these cases, a 10 to 20 Å compressive step produced a response that appeared to be a series of single layer–like events in which two or three layers were squeezed out. We found the net δd for these multiple events to be a multiple of 32 Å, in support of this view. This multiple-event dynamic response is rather remarkable, with a minimum $\delta d/\delta t$ between events that is much greater than the background $\delta d/\delta t$, and an event maximum $\delta d/\delta t$ that decreases rapidly for successive events, that is, with increasing $F_c - F$. Sucking-in events exhibit a threshold F and a characteristic dynamic signature in response to dilative steps essentially identical to that for squeezing-out events, implying some similarity between the dynamical processes of removing and adding a layer.

These discrete layering events must arise from either edge or screw dislocations (*7*). Because the 8CB was in a spherical wedge, it must have contained a series of dislocation loops to accommodate the increase of $d(\rho) = d_{min} + \rho^2/2R$, with ρ, the distance from the SFA centerline, normal to both of the two cylindrical surfaces. It is natural then to try to understand the jumps in terms of nucleation and motion of edge dislocations. We first considered the possibility that the dislocations are unpinned. If this were the case,

F would be supported by the area having the radius of the smallest loop, $\rho_1 = (2Ra)^{1/2} \cong 9\ \mu m$. Then K_{LC}, for a smectic A layer compressibility $B \sim 10^8$ dynes/cm^2 (16), would be $K_{LC} < 2.4 \times 10^6$ dynes/cm so that the LC layer would appear to be much softer than the external spring. The experiment indicates, however, that $K_{LC} > 2 \times 10^8$ dynes/cm, so we are in fact in the opposite limit, indicating that a much larger area ($\sim 100\pi\rho_1^2$), of radius $\rho > 100\ \mu m$, is resisting F. Therefore, the edge dislocations must be largely pinned at this temperature and applied stress.

Given this result, we developed models of the single-layer jump events based on the unpinning of edge dislocations, which must depend on achieving a critical value of applied stress (20). These models did not explain the data even qualitatively, exhibiting neither the observed avalanche-like dynamics nor the single-layer–sized jumps found for a range of values of F_c, for reasons which can be stated quite simply. The basic driving force for edge dislocation motion is stress, which falls as $\sim\rho^2$. Therefore, when the threshold stress for motion is reached in the center, the stress would be far below threshold for large ρ. The center of the LC film ($\rho < \rho_1$) can be the only part of the LC responsible for the definition of the jumps as single-layer events, but it carries only a small fraction of F. In this case the resulting net displacement would be much smaller than the layer thickness. Furthermore, once the dislocation begins to move it would relax stress, σ, so that $\delta d/\delta t$ would rise quickly to a sharp maximum at the opening of the loop and then decrease monotonically, which is contrary to observations.

The observation of a net displacement comparable with the layer thickness indicates that the jumps are caused by an instability that occurs at nearly the same time everywhere in the sample area. This observation suggests a mechanism that depends on applied dilation δd (which is independent of ρ) rather than applied stress or strain (which decreases rapidly with ρ). The work by Kléman *et al.* (10, 11) provides such a mechanism and prompted us to study the role of screw dislocation lines (SDLs), which are abundant in equilibrium 8CB (11, 21), by means of a Monte Carlo computer simulation of the dynamic response of a sample having the same geometry as ours. In an unstressed sample, the SDLs (●–●) are taken to run along the layer normal (z) direction (Fig. 2A) and to be attached to the bounding surfaces (11). Under layer normal stress, either compressive or dilative, a SDL can reduce stress by distorting into a helix (Fig. 2B): within the helix radius r, the number of layers between the plates is changed by n, where the helix pitch $p_n = d(\rho)/n$, which is less than 0 if the helix and SDL have the same handedness (10). As r increases, the angle between the defect line and z increases so that in the limit $r \gg p$ the screw dislocation line rotates into the layer plane becoming an edge dislocation (Fig. 2C). The SDL helixing can thus be viewed as an alternative mechanism for nucleating edge dislocations. SDL pairs (Fig. 2D) can also be generated by stress.

In the computer simulation a homeotropic smectic A of elliptical cross section, minor and major radii ρ_{min} and ρ_{maj}, and thickness $d(\rho)$ is assumed to contain a lattice of SDLs of Burgers' vector $\mathbf{b} = 1$, located on a rectangular lattice. The energy of a helixed line, $W(r)$, is a sum of core, self, and stress relaxation terms (10). For small δd, $W(r) \sim r^2$, and W_{max}, the maximum in $W(r)$, is at very large r. In this limit, the linear SDLs are stable. For large δd, $W(r) \sim -r^2$, W_{max} occurs at $r = 0$, and the linear SDLs are unstable, deforming spontaneously into helices. For intermediate δd, the core and self energy dominate at low r but the stress energy dominates at large r, producing a $W(r)$ with a W_{max} that can be comparable with the thermal energy k_BT (k_B is the Boltzmann constant), enabling the thermal generation of SDLs. The crucial characteristic that makes a cascade possible is that, whereas W_{max} of $W(r)$ is a very strong function of δd, it is nearly independent of $d(\rho)$, decreasing only slightly with increasing ρ. In the simulation, once a thickness change δd is imposed on the sample, the instability of each SDL is determined, with a Monte Carlo routine, by $P_t = \omega_1 \exp[-W_{max}/k_BT]$, the helix nucleation probability per unit time, where ω_1 is the frequency for the fundamental vibration of the dislocation line with ends fixed at the surfaces (10). After nucleation, the unit cell surrounding the lattice point is assumed to contain one less layer, that is, the helix is assumed to encompass the unit cell and become pinned at its boundary. Eventually, as the edge character becomes more pronounced, the repulsive image forces of the boundaries (7, 21) should push the coils of the line into the center where the loops will pinch off or annihilate with neighbors to form an edge dislocation surrounding a straight screw dislocation once again.

Simulations were carried out for $n \times n$ SDL arrays, with $6 \leq n \leq 100$, and various sized elliptical smectic A droplets, yielding single relaxation events that reproduce the main experimental features. The upper cylinder motion and the corresponding configuration of the helix array from a simulation run are shown in Fig. 2, E and F. The initial slow acceleration is caused by the helixing of a few of the SDLs at small ρ. The stress relieved over the area of a growing helix is

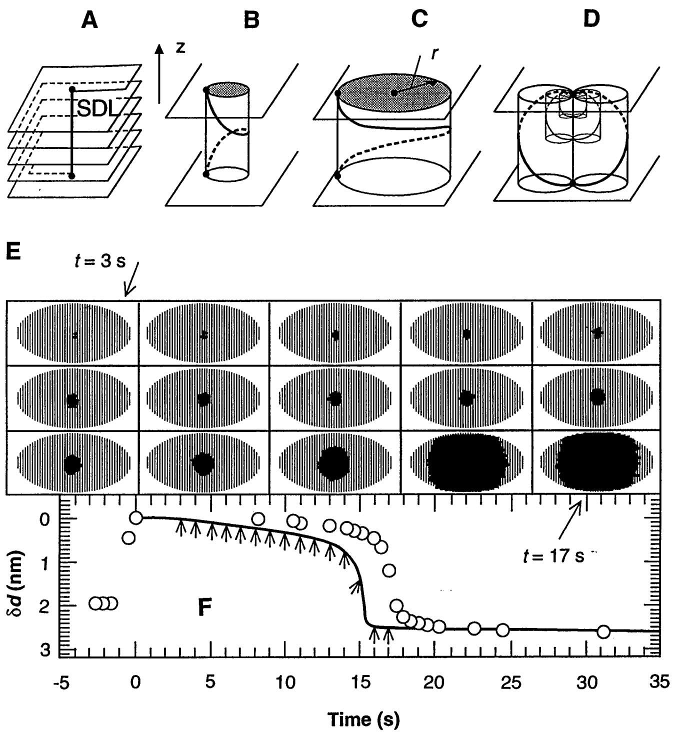

Fig. 2. (**A**) Smectic A screw dislocation line (●–●). The order parameter phase advances by 2π with each circuit around the core (vortex line). (**B**) Helixing instability of the screw dislocation under compressive stress (10, 11). One layer is removed between the plates in the shaded area. (**C**) As the radius r of the helix grows, the line rotates toward the layer plane, becoming more like an edge dislocation. (**D**) Helixed SDL pairs generated by stress. (**E**) Simulated time evolution of a single layer squeezing-out event arising from a helixing avalanche in a 25 × 25 SDL array after a compressive step $\delta d = -84.6$ Å at $t = 0$, showing lattice configurations at from 3 to 17 s corresponding to times indicated by arrows in (F). The helixed SDLs (black area of increasing size) appear first near the center ($\rho = 0$), initially increasing slowly in number and producing a slowly decreasing sample thickness [δd in (F)]. The decrease in d enhances the probability that remaining SDLs will helix, leading to an outward traveling wave of helixing and a jump in δd. (**F**) The $\delta d(t)$ for the simulated event in (D). The curve of open circles (O) depicts an experimental layer squeezing-out event at $d_{min} = 4\ \mu m$. For this simulation, $d_{min} = 4\ \mu m$, $p = 1$, $n = 1$, $\rho_{min} = 0.8$ mm, and $\rho_{maj} = 1.6$ mm.

distributed to the rest of the sample which increases δd and P_t for the rest of the SDLs, providing the basic mechanism for the cascade which finally moves out from the center of the sample as a well-defined front of helixing SDLs. The shape of the tail of the relaxation is determined by the drop elliptical shape, with slower relaxations when the range of ρ determining the drop boundary varies over a larger range. Although the precise value of $\delta d/\delta t$ at any point in the step depends on the exact size and shape of the LC sample, the qualitative features exhibited are relatively constant.

To model the multiple layer events shown in Fig. 1C, we assumed that some fraction (~10%) of the SDLs undergo multiple nucleations, an assumption which also tends to improve the qualitative correspondence of the single-step simulations to the experimental data. When one smectic A layer has been removed from nearly the entire sample, the dilation in the center, due to the multiply nucleated SDLs, is slightly greater than what it was initially, and the process quickly begins again. The multiply nucleated SDLs will not ordinarily undergo a second instability because the dilation in this area was already relieved by more than one layer, greatly reducing the nucleation probability. Thus, because of the lower average force and therefore dilation at the time of each second helical instability, this second step is significantly slower.

We have studied phase slippage events in the layering order parameter $\phi(\mathbf{r})$ of a smectic A in a thin spherical wedge. At temperatures well below the nematic–smectic A phase transition, a screw dislocation–mediated process appears at stresses below the threshold for unpinning of the edge dislocations present in the wedge geometry. The data indicate a threshold depending principally on net order parameter phase change (not strain or stress). In the spherical wedge, a weak residual dependence on stress produces an instability of screw dislocation helixing beginning in the cell center, where the stress is highest, and proceeding with an avalanche-like front to the thicker part of the wedge.

REFERENCES AND NOTES

1. P. G. deGennes and J. Prost, *The Physics of Liquid Crystals* (Clarendon, Oxford, ed. 2, 1993); B. S. Chandrasekhar, *Liquid Crystals* (Cambridge Univ. Press, Cambridge, ed. 2, 1993).
2. R. G. Horn, J. N. Israelachvili, E. Perez, *J. Phys.* (*Paris*) **42**, 39 (1981).
3. P. Kékicheff and H. K. Christenson, *Phys. Rev. Lett.* **63**, 2823 (1989).
4. P. Richetti *et al.*, *Nature* **346**, 252 (1990).
5. J. N. Israelachvili, *Intermolecular & Surface Forces* (Academic Press, London, 1992).
6. P. G. deGennes, *Solid. State Commun.* **10**, 753 (1972).
7. M. Kléman, *Points, Lines, and Walls* (Wiley, New York, 1983).
8. W. I. Glaberson, W. W. Johnson, R. M. Ostermeir, *Phys. Rev. Lett.* **33**, 1197 (1974).
9. J. R. Clem, *ibid.* **38**, 1427 (1977).
10. L. Bourdon, M. Kléman, L. Lejcek, D. Taupin, *J. Phys.* (*Paris*) **42**, 261 (1981).
11. P. Oswald and M. Kléman, *ibid.* **45**, L319 (1984).
12. P. P. Karat and N. V. Madhusudana, *Mol. Cryst. Liq. Cryst.* **36**, 51 (1976).
13. R. Herke, N. A. Clark, M. A. Handschy, unpublished results; R. Herke, thesis, University of Colorado (1993).
14. D. Davidov *et al.*, *Phys. Rev. B* **19**, 1657 (1979).
15. G. B. Kasting *et al.*, *J. Phys.* (*Paris*) **41**, 879 (1980); J. Thoen *et al.*, *Phys. Rev. A* **26**, 2886 (1982).
16. M. R. Fisch *et al.*, *Phys. Rev. A* **29**, 2741 (1984); M. Benzekri *et al.*, *Phys. Rev. Lett.* **68**, 2480 (1992).
17. N. A. Clark, *Phys. Rev. A* **14**, 1551 (1976).
18. R. Ribotta and G. Durand, *J. Phys.* (*Paris*) **38**, 179 (1977); R. Bartolino and G. Durand, *Phys. Rev. Lett.* **39**, 1346 (1977).
19. R. A. Herke, N. A. Clark, M. A. Handschy, data not shown.
20. F. R. N. Nabarro, *Theory of Crystal Dislocations* (Dover, New York, 1967).
21. M. Kléman, *J. Phys.* (*Paris*) **35**, 595 (1974).

22. This work supported by NSF Solid State Chemistry Grant DMR 92-23729.

13 July 1994; accepted 21 November 1994

Imaging with Intermolecular Multiple-Quantum Coherences in Solution Nuclear Magnetic Resonance

Wolfgang Richter, Sanghyuk Lee, Warren S. Warren,* Qiuhong He

A magnetic resonance imaging technique based on intermolecular multiple-quantum coherences in solution (the correlated spectroscopy revamped by asymmetric *z* gradient echo detection or CRAZED experiment) is described here. Correlations between spins in different molecules were detected by magnetic-field gradient pulses. In order for a correlation to yield an observable signal, the separation between the two spins must be within a narrow band that depends on the area of the gradient pulses. The separation can be tuned from less than 10 micrometers to more than 1 millimeter, a convenient range for many applications.

A variety of nuclear magnetic resonance (NMR) methods have proven useful for extracting structural information. For example, the nuclear Overhauser effect (NOE) (*1*) can be used to determine if two spins are within approximately 5 Å and is crucial for the determination of macromolecular structure. On a much larger scale (millimeters), the internal structure of a sample can be conveniently mapped by magnetic resonance imaging (MRI) (*2*, *3*). The spatial resolution in MRI arises from gradient pulses, which cause spins to evolve at different frequencies in different sample positions; increasing the gradient strength improves the spatial resolution. However, the most important resolution limitation in three-dimensional imaging is not the strength of the gradient pulse. Improving spatial resolution by a factor of 2 decreases the number of spins in each voxel by a factor of 8, and eventually sensitivity considerations dominate. Thus, in practice, imaging with 10-μm resolution is quite challenging.

Here, we show direct experimental evidence of the spatial selectivity of the CRAZED experiment with a set of phantoms. This experiment (Fig. 1) is a conventional correlated spectroscopy (COSY) experiment, modified with an *n*-quantum gradient filter at the second pulse. Our results verify the theoretical model presented by Warren and co-workers (*4*, *5*), which predicted that it should be possible to observe cross peaks between separated samples, but only if the separation is smaller than the pitch of the magnetization helix generated by the gradient pulses. Thus, changing the gradient pulse strength couples or decouples the separated samples. We also discuss the possible application of this approach as an imaging technique.

According to the prevailing theory (*1*, *6*), the CRAZED pulse sequence cannot generate any observable magnetization; the first pulse could merely produce single-quantum coherences, I_x, which would be dephased by the gradient filter unless $n = 1$. However, application of this pulse sequence (with $n = 2$, for example) to a concentrated sample led to observable double-quantum transitions in the indirectly detected dimension (F_1) and single-quantum transitions in the directly detected dimension (F_2). The conclusion was that double-quantum, two-spin coherences must be present after the first pulse in order to evolve in time t_1, and

W. Richter, S. Lee, W. S. Warren, Department of Chemistry, Princeton University, Princeton, NJ 08544, USA.
Q. He, Department of Radiology, NMR Research Division, Johns Hopkins University School of Medicine, Baltimore, MD 21205, USA.

*To whom correspondence should be addressed.